Computers and Concrete, *Vol. 23, No. 4 (2019) 235-243*
DOI: https://doi.org/10.12989/cac.2019.23.4.235

The continuous-discontinuous Galerkin method applied to crack propagation

Tiago L.D. Forti[*1], Nadia C.S. Forti[2a], Fábio L.G. Santos[1b] and Marco A. Carnio[3c]

[1] *Simworx R&D, Campinas-SP, Brazil*
[2] *Pontifical Catholic University of Campinas, Campinas-SP, Brazil*
[3] *Evolução Engenharia, Valinhos-SP, Brazil*

(Received October 30, 2018, Revised March 12, 2019, Accepted March 21, 2019)

Abstract. The discontinuous Galerkin method (DGM) has become widely used as it possesses several qualities, such as a natural ability to dealing with discontinuities. DGM has its major success related to fluid mechanics. Its major importance is the ability to deal with discontinuities and still provide high order of approximation. That is an important advantage when simulating cracking propagation. No remeshing is necessary during the propagation, since the crack path follows the interface of elements. However, DGM comes with the drawback of an increased number of degrees of freedom when compared to the classical continuous finite element method. Thus, it seems a natural approach to combine them in the same simulation obtaining the advantages of both methods. This paper proposes the application of the combined continuous-discontinuous Galerkin method (CDGM) to crack propagation. An important engineering problem is the simulation of crack propagation in concrete structures. The problem is characterized by discontinuities that evolve throughout the domain. Crack propagation is simulated using CDGM. Discontinuous elements are placed in regions with discontinuities and continuous elements elsewhere. The cohesive zone model describes the fracture process zone where softening effects are expressed by cohesive zones in the interface of elements. Two numerical examples demonstrate the capacities of CDGM. In the first example, a plain concrete beam is submitted to a three-point bending test. Numerical results are compared to experimental data from the literature. The second example deals with a full-scale ground slab, comparing the CDGM results to numerical and experimental data from the literature.

Keywords: finite elements; discontinuous Galerkin; cracking propagation; cohesive fracture; concrete; steel-fiber reinforced concrete

1. Introduction

Many engineering problems are formulated as boundary value problems for second order elliptic differential equations. Elasticity, diffusion, heat conduction, Darcy's flow are examples of phenomena modeled by second order elliptic problems.

The finite element method (FEM) approximates the solution of partial differential equations based on the Galerkin method using a systematic way of generating subspaces or subset of approximating functions. Different finite element formulations have been developed to solve second-order elliptic problems. In fact, the expression finite element refers to a broad family of methods such as continuous, discontinuous Galerkin, mixed methods, hybrid methods, among others. Thus, before solving an engineering problem, one needs to choose the formulation that is more suited to the kind of application at hand. That choice would be guided by different aspects concerning the quantity of interest. Depending on whether the application aims to compute the solution or the flux field, it would determine the choice of a primal or a mixed H(div)-conforming formulation (Forti *et al.* 2016). Other concerns relate to local conservation property, ability to deal with solution discontinuities, etc.

The discontinuous Galerkin finite element method (DGM) (Oden *et al.* 1998, Süli *et al.* 2000, Cangiani *et al.* 2014) has become widely used as it possesses several qualities, such as: flexible mesh design as hanging nodes are admissible; easy implementation of *hp*-adaptive algorithms; a natural ability to deal with discontinuities; the accuracy is obtained by means of high-order polynomials within elements, without any regularity constraint at element interfaces. Furthermore, unstructured meshes and parallelization can be easily handled. The combination of these properties leads to robust solvers with high precision in space and wide stability range.

These properties however come with the drawback of an increased number of degrees of freedom. It means that discontinuous Galerkin is more accurate and stable solving problems with discontinuities but more costly than the classical continuous H^1 finite element method. With this motivation, it seems a natural approach to combining both continuous and discontinuous elements in the same simulation obtaining the advantages of both methods. This

∗Corresponding author, Research Engineer
E-mail: forti@simworx.com.br
[a]Professor
E-mail: nadia.cazarim@puc-campinas.edu.br
[b]Research Engineer
E-mail: gea@simworx.com.br
[c]Civil Engineer
E-mail: mac@evengenharia.com.br

http://www.techno-press.org/?journal=cac&subpage=8
ISSN: 1598-8198 (Print), 1598-818X (Online)

approach was employed by Clint Dawson and Proft (2002), Devloo *et al* (2007), Cangiani *et al.* (2013). Following that strategy, discontinuous elements are placed in regions where the solution has discontinuities and continuous elements are adopted elsewhere, where the solution is smooth.

The control of discontinuities across element interfaces in DGM can be adjusted by using the so-called jump penalization. Using excessive penalization within a DGM approximation is referred as the super penalty method (Cangiani *et al.* 2014).

An important problem in engineering is the simulation of crack propagation in concrete structures or rocks (Gamino *et al.* 2010, Elsaigh *et al.* 2011, Yaylaci 2016, Kh *et al* 2016, Shaowei *et al* 2016, Lin *et al.* 2017, Feng and Wu 2018, Suárez *et al.* 2019, Kurumatani *et al.* 2019). Concrete is a very versatile material, applied in different types of constructions around the world. Advantages of this material is its ability to mold complex shapes, its fire resistance, and resistance to atmospheric conditions providing the structure the necessary durability. Economic factors also contribute to the wide use of concrete structures. However, its mechanical behavior is complex. One difficult in modeling concrete structures is the definition of constitutive laws that are able to describe its non-linear behavior and the process of cracking. Concrete is a material with low tensile resistance and many internal micro defects and micro cracks exist even before any loading is applied (Santos and Souza 2015). The mechanical behavior is strongly influenced by the initiation and propagation of these internal microcracks. The problem is characterized by a discontinuity (or several discontinuities) that evolves throughout the domain as external loads are applied. In this work, it is proposed to employ the combined continuous-discontinuous Galerkin method (CDGM) to simulate crack propagation in concrete structures.

The work is organized as follows. Section 2 presents the formulation of CDGM for the 3D elasticity problem and discusses the cohesive fracture theory for describing crack propagation. Section 3 describes the algorithm adopted to solve the crack propagation problem. Numerical examples are presented in Section 4. The first one is a three-point bending test where numerical results are compared to published experimental data. Second example describes the application of the CDGM to a full-scale steel-fiber reinforced concrete ground slab. Section 5 concludes the paper.

2. Formulation

This section describes the formulation of the combined continuous-discontinuous Galerkin method (CDGM) for the 3D elasticity problem. The elasticity problem is given by the equilibrium equation

$$div(\overleftrightarrow{\sigma}) + \vec{b} = \vec{0}, in\ \Omega$$

where $\overleftrightarrow{\sigma}$ is the Cauchy stress tensor, $\vec{b} = \{b_x, b_y, b_z\}^T$ are body forces, and $\Omega \subset \mathbb{R}^3$ is a bounded domain with boundary $\partial\Omega$. Each component of $\vec{b}$ is a function in $L^2(\Omega)$, the space of square-integrable functions. The stress tensor is given, in linear elasticity, by the constitutive law

$$\overleftrightarrow{\sigma} = \begin{pmatrix} \sigma_{xx} & \tau_{xy} & \tau_{xz} \\ \tau_{xy} & \sigma_{yy} & \tau_{yz} \\ \tau_{xz} & \tau_{yz} & \sigma_{zz} \end{pmatrix} = \lambda\, tr(\overleftrightarrow{\epsilon})\, \overleftrightarrow{I} + 2\, G \overleftrightarrow{\epsilon}$$

where $\overleftrightarrow{\epsilon}$ is the strain tensor and λ and G are the Lamé's coefficients, related to the Young's module E and Poisson coefficient ν by the following expressions

$$\lambda = \frac{\nu\, E}{(1+\nu)(1-2\nu)}$$

$$G = \frac{E}{2(1+\nu)}$$

The infinitesimal strain tensor is given by

$$\overleftrightarrow{\epsilon} = \begin{pmatrix} \epsilon_{xx} & \epsilon_{xy} & \epsilon_{xz} \\ \epsilon_{xy} & \epsilon_{yy} & \epsilon_{yz} \\ \epsilon_{xz} & \epsilon_{yz} & \epsilon_{zz} \end{pmatrix} = \frac{1}{2}(\nabla\vec{u} + \nabla\vec{u}^T)$$

where $\vec{u} = \{u_x, u_y, u_z\}^T$ is the displacement field.

Boundary conditions can be prescribed displacements (Dirichlet type) or external forces (Neumann type) and a same boundary region can have both types, i.e., a prescribed displacement in x and y direction and an external force in z direction, for instance. A general description can be expressed by a mixed boundary condition in the form

$$\overleftrightarrow{\sigma} \cdot \vec{n} = M(\vec{u} - \vec{u}_0) + \vec{g}, in\ \partial\Omega$$

where M is a matrix of scalars and $\vec{u}_0$ and $\vec{g}$ are given functions with each component a function in $L^2(\Omega)$.

2.1 Continuous finite element formulation

The classical H^1 formulation (Oden *et al.* 1981) is stated as: find $\vec{u} \in U(\Omega)$ such that

$$\int_\Omega \overleftrightarrow{\sigma} : \nabla\vec{w}\, d\Omega = \int_\Omega \vec{w} \cdot \vec{b}\, d\Omega + \\ + \int_{\partial\Omega} \vec{w} \cdot (M(\vec{u} - \vec{u}_0) + \vec{g})\, d\omega \quad \forall\vec{w} \in U(\Omega), \tag{1}$$

where

$$U(\Omega) = [H^1(\Omega)]^3 = \{\vec{v} = \{v_1, v_2, v_3\}^T : v_i \in H^1(\Omega), \\ i = 1,2,3\}$$

$$H^1(\Omega) = \left\{v \in L^2(\Omega); \frac{\partial v}{\partial x_i} \in L^2(\Omega), i = 1,2,3)\right\}$$

2.2 Discontinuous Galerkin formulation

The discrete version for the discontinuous Galerkin weak formulation (Oden *et al.* 1998) is constructed over the broken polynomial space

$$V_p(\Pi_h) = \{\vec{v} = \{v_1, v_2, v_3\}^T : v_i \in L^2(\Omega); v_i|_{\Omega_e} \\ \in P_p(\Omega_e), \forall\Omega_e \in \Pi_h\ , i = 1,2,3\}$$

where Π_h is a partition of the domain Ω,

$$\Pi_h = \{\Omega_e, e = 1, \dots, nel\},$$

and Ω_e are open subsets with $\Omega = \bigcup_{e=1}^{nel} \bar{\Omega}_e$, nel is the number of elements, and $\Omega_e \cap \Omega_i = \emptyset$ for $e \neq i$. $P_p(\Omega_e)$ are locally defined polynomial spaces of maximum degree p. We also adopt the notation $\Gamma_{\Pi_h} = \partial\Omega \cup \Gamma_{int}$, where Γ_{int} is the union of all interelement boundaries. If elements Ω_e and Ω_f have a common inter-element boundary Γ_{ef}, the normal vector $\vec{n}$ is defined as $\vec{n} = \vec{n}_f = \vec{n}_e$, with $e > f$, being n_e the outward normal of the boundary $\partial\Omega_e$. Thus, the discrete weak formulation is given as: find $\vec{u} \in V_p(\Pi_h)$ such that

$$\begin{aligned} &\sum_{e=1}^{nel} \left\{ \int_{\Omega_e} \overleftrightarrow{\sigma} : \nabla\vec{w}\, d\Omega_e \right\} + \\ &+ \int_{\Gamma_{int}} (\theta\langle \overleftrightarrow{\sigma}_w . \vec{n}\rangle \cdot [\vec{u}] - \langle \overleftrightarrow{\sigma} . \vec{n}\rangle \cdot [\vec{w}]) d\omega + \\ &+ \int_{\Gamma_{int}} \gamma\, [\vec{u}] \cdot [\vec{w}]\, d\omega = \sum_{e=1}^{nel} \left\{ \int_{\Omega_e} \vec{w} \cdot \vec{b}\, d\Omega_e \right\} + \\ &+ \int_{\partial\Omega} \vec{w} \cdot (M(\vec{u} - \vec{u}_0) + \vec{g})\, d\omega \end{aligned} \tag{2}$$

for any $\vec{w} \in V_p(\Pi_h)$, where

$$\overleftrightarrow{\sigma}_w = \lambda\, \mathrm{tr}\left(\frac{1}{2}(\nabla\vec{w} + \nabla\vec{w}^T)\right) \overleftrightarrow{I} + 2\, G\left(\frac{1}{2}(\nabla\vec{w} + \nabla\vec{w}^T)\right),$$

$\langle \overleftrightarrow{\sigma} \cdot \vec{n}\rangle$ and $[\vec{w}]$ are the average and jump operators

$$\langle \overleftrightarrow{\sigma} \cdot \vec{n}\rangle = \frac{\overleftrightarrow{\sigma}_e \cdot \vec{n} + \overleftrightarrow{\sigma}_f \cdot \vec{n}}{2},$$
$$[\vec{w}] = \vec{w}|_{\partial\Omega_e} - \vec{w}|_{\partial\Omega_f}$$

which are defined between two elements Ω_e and Ω_f, with $e > f$, having a common boundary Γ_{ef}. By setting $\theta = +1$, one would obtain the non-symmetric interior penalty formulation (Oden *et al.* 1998). By setting $\theta = -1$, a symmetric formulation is obtained. Parameter $\gamma > 0$ is the jump penalization parameter.

The control of discontinuities across element interfaces can be exercised by tuning the value of γ. Using excessive penalization is referred as the super penalty method (Cangiani *et al.* 2014). It is natural to expect that as the value of γ increases the interelement jumps in the numerical approximation decrease. Larson and Niklasson (2001) showed that the discontinuous approximation converges to the classical H^1 approximation as the jump penalization parameter tends to infinity. Thus, it is proposed to simplify the DGM formulation presented in Eq. (2). In Eq. (2), there are two integral across interfaces: the natural DGM flux, given by

$$F_N = \int_{\Gamma_{int}} (\theta\langle \overleftrightarrow{\sigma}_w \cdot \vec{n}\rangle . [\vec{u}] - \langle \overleftrightarrow{\sigma} \cdot \vec{n}\rangle \cdot [\vec{w}]) d\omega$$

and the penalty flux given by

$$F_\gamma = \int_{\Gamma_{int}} \gamma\, [\vec{u}] \cdot [\vec{w}]\, d\omega.$$

When super penalization is adopted the natural flux loses its numerical importance compared to the penalty flux. Therefore, Eq. (2) could be simplified by neglecting the natural DGM flux and the formulation is then stated as: find $\vec{u} \in V_p(\Pi_h)$ such that

$$\begin{aligned} &\sum_{e=1}^{nel} \left\{ \int_{\Omega_e} \overleftrightarrow{\sigma} : \nabla\vec{w}\, d\Omega_e \right\} + \int_{\Gamma_{int}} \gamma\, [\vec{u}] \cdot [\vec{w}]\, d\omega = \\ &= \sum_{e=1}^{nel} \left\{ \int_{\Omega_e} \vec{w} \cdot \vec{b}\, d\Omega_e \right\} + \int_{\partial\Omega} \vec{w} \cdot (M(\vec{u} - \vec{u}_0) + \vec{g})\, d\omega \end{aligned} \tag{3}$$

for any $\vec{w} \in V_p(\Pi_h)$. A drawback of this simplified formulation is that exact solutions could never be achieved since there will always be a discontinuity across elements. However, the discontinuity can be reduced to any required precision by properly tuning the super penalization parameter γ.

2.2.1 Selection of the jump super penalization parameter

The selection of the jump super penalization parameter is motivated by a physical argument. In a one dimensional problem where the stress state is a constant tension of value σ_{xx} the longitudinal strain ϵ_{xx} is computed as $\epsilon_{xx} = \frac{\sigma_{xx}}{E}$ and the elongation of a finite element of size h is $\delta u = \epsilon_{xx}\, h = \frac{\sigma_{xx}}{E}\, h$. An interface connecting two neighbor elements of size h, each one presenting an elongation of $\delta u = \frac{\sigma_{xx}}{E}\, h$, would have a jump $[u]$ given by

$$[u] = \frac{\sigma_{xx}}{\gamma}$$

This discontinuity is not part of the exact solution and, therefore, should be minimal. A trivial conclusion is to adopt the highest possible value for γ, but that would introduce numerical errors that could eventually spoil the approximate solution. Thus, it is proposed to search γ such that $[u] < \alpha\, 2\, \delta u$, with $\alpha \ll 1$, limiting the influence of $[u]$ in the approximate solution. Then, we have

$$[u] = \frac{\sigma_{xx}}{\gamma} < \alpha\, 2\, \delta u$$
$$[u] = \frac{\sigma_{xx}}{\gamma} < \alpha\, 2\, \frac{\sigma_{xx}}{E}\, h$$
$$\gamma > \frac{E}{\alpha\, 2h}$$

obtaining an expression to γ which is a function of α. In consequence, one can choose the value of α ($\alpha = 10^{-3}$, $\alpha = 10^{-6}$ etc) and obtain the adequate value of γ. For instance, by choosing $\alpha = 10^{-3}$, the impact of the interface discontinuity will represent only 0.1% of the total elongation. Moreover, the expression is function of the element size h and therefore is compatible to mesh refinement. This expression is in accordance to the usually adopted values in the literature (Süli *et al.* 2000), which also includes the square of the polynomial order of approximation p, resulting in

$$\gamma = \frac{E\,p^2}{\alpha\,2h}.$$

For hp adaptive meshes, the expression assumes the form

$$\gamma = \frac{E < p^2 >}{\alpha\,(h_e + h_f)}$$

where $< p^2 > = \frac{1}{2}(p_e^2 + p_f^2)$, p_e and p_f the approximation order of neighbor elements e and f, and h_e and h_f are their characteristic size.

2.2.2 Cohesive fractures

The adequate and careful choice of the model is determinant to the success of the finite element simulation of cracking propagation in concrete structures. An aspect of major importance is describing the crack and the mechanical behavior of the cracked material. Traditionally, three lines of research have been developed: discrete, distributed and embedded cracks.

In the discrete crack modeling, cracks are modeled as displacement discontinuities between elements. These models are based in the idea of simulating only the continuous and non-damaged part of the domain while cracks form the boundary of the domain. Then, the cracks develop and propagate following the boundary of elements, which impose a restriction to their propagation path. Remeshing or h_p adaptivity technologies aim to better describe the path of cracking.

The fictitious crack model or cohesive zone model describes the fracture process zone as a discrete crack (fictitious) where softening effects are expressed by cohesive zones in the interface of elements (Barenblatt 1962, Barenblatt 1959, Hillerborg *et al.* 1976, Asferg *et al.* 2007, Yu *et al.* 2008, Dong *et al.* 2010, and Murthy *et al.* 2015). The crack formation is considered as a gradual phenomenon. Initially, the material is under linear elastic stress. After reaching a certain tension stress value, crack starts to open. Then, an inelastic process takes place until the crack aperture reaches a critical value and the crack faces are completely separated. The cohesive stress is defined as function of the relative displacement (or crack aperture) $[u]$. Fig. 1 illustrates a cohesive curve. The cohesive model fits the proposed discontinuous Galerkin formulation and the penalty flux is changed to

$$F_\gamma = \int_{\Gamma_{int}} (1 - D)\,\gamma\,[\vec{u}] \cdot [\vec{w}]\,d\omega$$

where D stands for a damage coefficient $D = (0,1)$ which is function of the normal aperture $[u_n] = [\vec{u}] \cdot \vec{n}$. The damage coefficient D reduces the cohesive stresses as the crack aperture evolves. Fig. 2 helps illustrating the calculation of the damage coefficient D. Initially, crack has not initiated and a linear elastic behavior is observed with $D = 0$. After the normal stress reaches the concrete tension strength f_t, the cohesive stresses govern the problem and the damage value is $D > 0$. Taking point 1 of Fig. 2, we

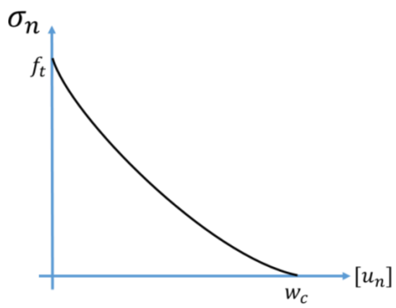

Fig. 1 Example of cohesive curve

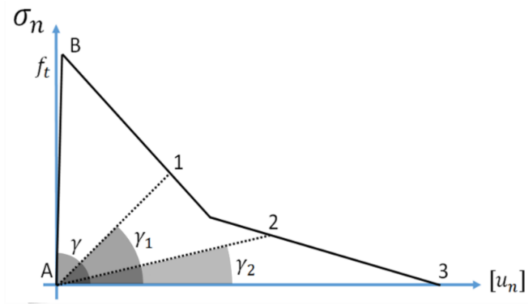

Fig. 2 Example of a numerical cohesive curve

have $\sigma_n^1 = \gamma_1[u_n] = (1 - D_1)\,\gamma\,[u_n]$ from where we obtain the value of D_1.

The straight line from point A to B in Fig. 2 represents the penalty formulation from the DGM. Thus, it is important that this straight line be limited to the very beginning of the cohesive curve.

The discontinuous Galerkin formulation is finally stated as: find $\vec{u} \in V_p(\Pi_h)$ such that

$$\sum_{e=1}^{nel}\left\{\int_{\Omega_e} \overleftrightarrow{\sigma} : \nabla\vec{w}\,d\Omega_e\right\} + \int_{\Gamma_{int}} (1 - D)\,\gamma\,[\vec{u}] \cdot [\vec{w}]\,d\omega =$$
$$= \sum_{e=1}^{nel}\left\{\int_{\Omega_e} \vec{w} \cdot \vec{b}\,d\Omega_e\right\} + \int_{\partial\Omega} \vec{w} \cdot (M(\vec{u} - \vec{u}_0) + \vec{g})\,d\omega$$

for any $\vec{w} \in V_p(\Pi_h)$.

The problem was formulated for mode I crack. Other modes could be easily included in the model. Then, the damage coefficient D would be function not only of the normal aperture, but also of the sliding relative displacements.

2.3 Continuous-discontinuous Galerkin formulation

The continuous-discontinuous Galerkin (CDGM) formulation is obtained by splitting the mesh into two regions. In one region, the continuous H^1 formulation is adopted. In the other region, the DGM is adopted. Coupling both regions is made by using the DGM flux between neighbor elements, in the same manner as the DGM. If we define Γ_{CD} as the union of all interface elements between the two mentioned regions, we have the penalty flux given by $F_\gamma^{CD} = \int_{\Gamma_{CD}} (1 - D)\,\gamma\,[\vec{u}] \cdot [\vec{w}]\,d\omega$. It couples the equations and allows the CDGM simulation.

3. Problem solving strategy

The problem is simulated by applying the external loads in sub steps. For each sub step, a non-linear problem has to be solved. The CDGM formulation is non-linear because the cohesive curve, which defines the penalty fluxes in Γ_{int} and Γ_{CD}, is function of the relative normal displacement of interface neighbors. Moreover, the numerical cohesive curve, as illustrated in Fig. 2, is not monotonic. There are two possible $[\vec{u}]\cdot\vec{n}$ values for a given normal stress. The first value is given while the material is in its linear elastic domain. The second one is given when softening is governing. Therefore, it is proposed to "flag" each integration point of interface elements with its state, which can be "linear" or "softening". Thus, the incremental load step is an important issue to capture the transition of "states" properly.

The algorithm can be summarized as

1. All integration points are flagged as "linear state"
2. Set the load step
3. Solve the non-linear problem
4. Update the state of integration points. If the normal stress at a given point is higher than the material tension strength, the point is flagged as "softening state".
5. If any point is changed to "softening state", go back to step 3
6. After converging the substep, post process solution: calculate support reactions and write plot files
7. Increment load step and go back to step 2 until the full load is applied.

The simulations were implemented in C++ language using the object-oriented scientific computational environment PZ (http://github.com/labmec/neopz). PZ is a general finite element approximation software, which incorporates a variety of element geometries, variational formulations, and approximation spaces. It contains modules for a broad classes of technologies such as system resolution, finite element geometric approximation, finite element approximation spaces (e.g., continuous, discontinuous, *H*(div), and others) and mesh adaptivity.

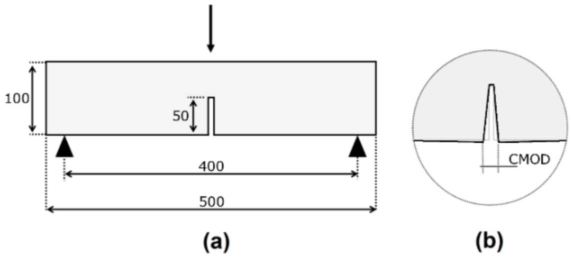

Fig. 3 Problem 1: (a) pre-notched beam (dimensions in mm); (b) definition of CMOD (crack mouth opening displacement)

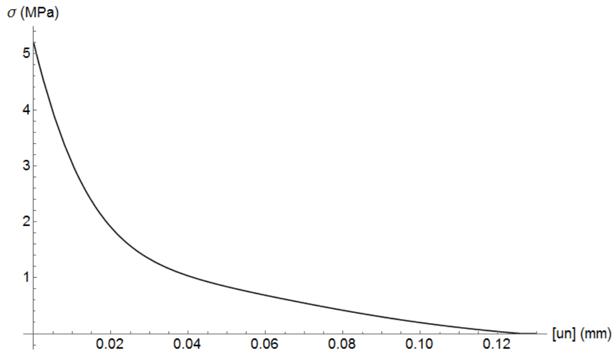

Fig. 4 Hordijk cohesive curve

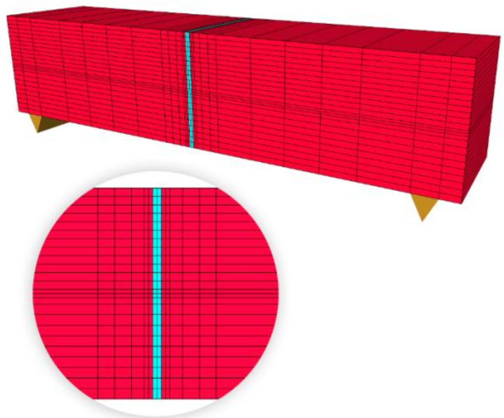

Fig. 5 Problem 1 mesh: perspective view of 3D elements and highlight of region with discontinuous (blue) and continuous elements (red)

4. Numerical experiments

4.1 Problem 1: Three-point bending test

The CDGM formulation is applied to solve a three-point bending test, illustrated in Fig. 3. The pre-notched beam has a cross-section width of 100 mm. The beam has a pinned support on the left and a roller support on the right. A vertical force is applied in the middle of the beam. The vertical force is actually imposed as a prescribed displacement δ and the reaction force P is read.

Numerical results are compared to experimental data from Rosa *et al.* (2012). The cohesive curve is defined using Hordijk's analytical equation (Hordijk 1991)

$$\sigma_{cohesive} = \mathrm{f_{tc}}\left(\left(1-\left(3\frac{\mathrm{w}}{\mathrm{w_{lt}}}\right)^3\right)\mathrm{e}^{-6.93\frac{\mathrm{w}}{\mathrm{w_{lt}}}} - 28\frac{\mathrm{w}}{\mathrm{w_{lt}}}\mathrm{e}^{-6.93}\right), \text{for } \mathrm{w} \le 5.136\frac{\mathrm{G_F}}{\mathrm{f_{tc}}};$$

$$\sigma_{cohesive} = 0, \text{otherwise.}$$

where $w_{lt} = 5.136\frac{G_F}{f_{tc}}$, f_{tc} is the concrete tension strength and G_F is the apparent fracture energy, corresponding to the amount of energy per unit area required for the complete separation of the two fracture faces. Rosa *et al.* (2012) found $G_F = 98\ \mathrm{J/m^2}$ and $f_{tc} = 5.2\ \mathrm{MPa}$. With these values, the cohesive curve is calculated and depicted in Fig. 4. Other parameters are the Young's module $E = 33900\ \mathrm{MPa}$ and Poisson coefficient $\nu = 0.2$.

This numerical problem adopts a mesh aligned with the path of the cracking and aim to reproduce the experimental results of Rosa et al. (2012).

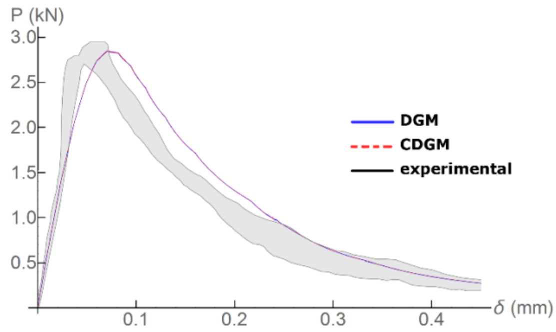

Fig. 6 Problem 1 $P-\delta$ results: DGM (blue line), CDGM (red dashed line) and experimental results range

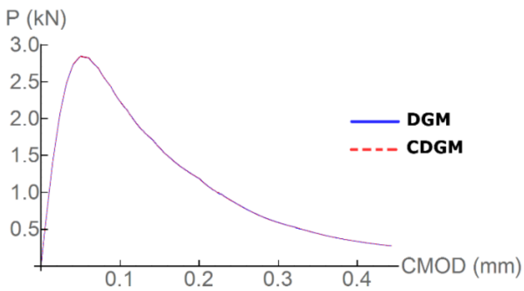

Fig. 7 Problem 1 P-CMOD results: DGM (blue line) and CDGM (red dashed line)

The problem adopts the mesh shown in Fig. 5. The crack is expected to initiate in the notch and propagate vertically. Since the mesh is perfectly aligned, only elements neighbor to the crack should be of discontinuous Galerkin type. Other elements can be continuous elements.

The problem was solved using the CDGM mesh shown in Fig. 5 and with a full DGM mesh. Approximation order $p = 1$ is adopted for all elements. A vertical displacement of 0.45 mm was applied within 10,000 steps of 0.000045 mm each. The jump penalization parameter $\gamma = \frac{E\,p^2}{\alpha\,2h}$ is set with $\alpha = 10^{-3}$.

Results are presented in Figs. 6, 7 and 8. Fig. 6 shows the curve of vertical force P versus the imposed vertical displacement δ. It compares the results obtained with both DGM and CDGM methods and the experimental data from Rosa *et al.* (2012). The numerical solutions present a peak

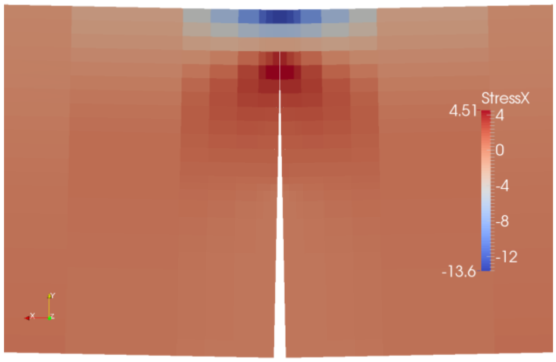

Fig. 8 Problem 1: deformed shape of CDGM solution at the vicinity of the crack for instant when $\delta = 0.14\,mm$. Deformation is scaled 30 times for better visualization

load similar to that of the experiments and a good agreement of late stages of loading. Results of the CDGM mesh and DGM are almost identical. Differences of $P(\delta)$ are less than 2% for all steps. However, their computational cost differ considerably: the CDGM mesh has 5,064 degrees of freedom while the DGM mesh has 15,012. Fig. 7 brings the curve of P versus $CMOD$ (crack mouth opening displacement) and Fig. 8 shows the deformed shape of the CDGM solution for the instant $\delta = 0.14\,mm$

4.2 Problem 2: Steel-fiber reinforced concrete ground slab

In this section, a steel-fiber reinforced concrete (SFRC) ground slab is simulated using the CDGM method. The problem is presented by Elsaigh *et al.* (2011), which presents both numerical and experimental results.

The full-scale SFRC ground slab was tested by Elsaigh (2001). The layout of the slab test is shown in Fig. 9. The SFRC contained 15 kg/m^3 of hooked end wires. The concrete has an average Young's modulus of 28 GPa and compressive strength of 45 MPa. A foamed concrete slab weighing 780 kg /m^3 supports the slab. Elsaigh *et al.* (2011) simulates the foamed concrete slab as part of their three dimensional domain. In this work, it was simulated as a non-tension spring boundary condition. The spring stress-displacement response is presented in Fig. 10. The spring

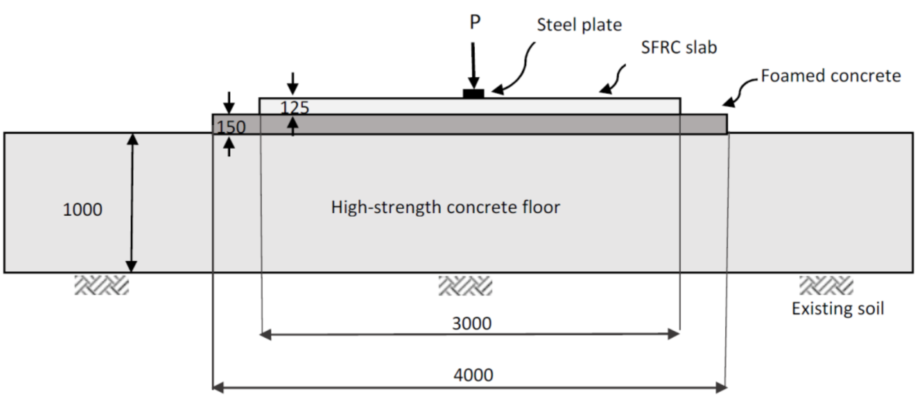

Fig. 9 Problem 2: Test layout

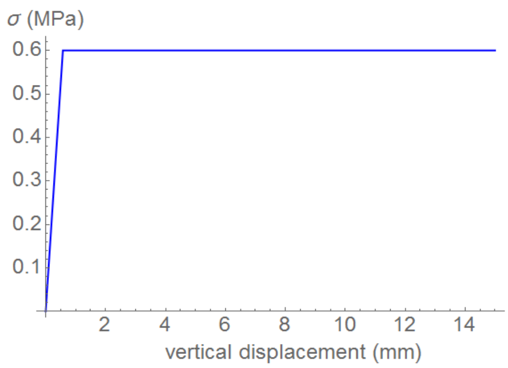

Fig. 10 Problem 2: No tension spring: stress-displacement response

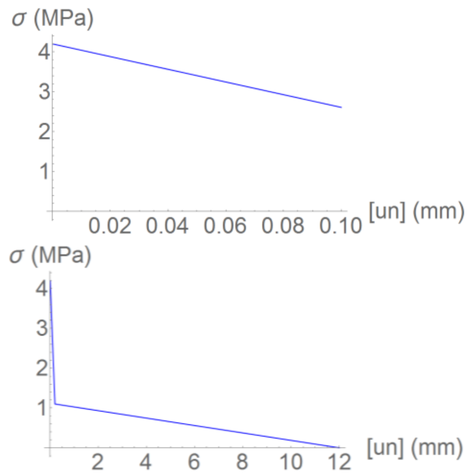

Fig. 11 Problem 2: cohesive bilinear curve (initial and full data). Data = {{0,4.2}, {0.195,1.1},{12,0}}

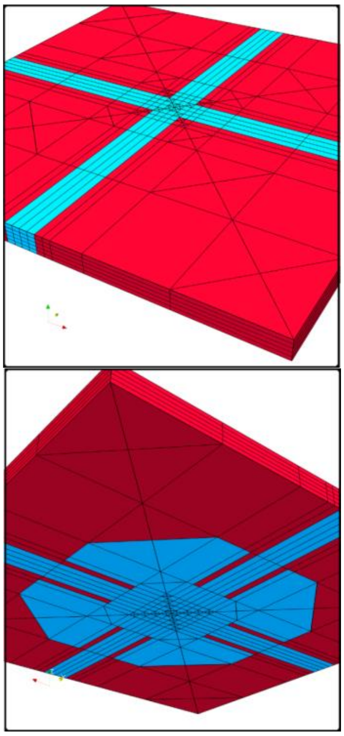

Fig. 12 Problem 2 mesh (top and bottom view): discontinuous elements are blue; continuous elements are red

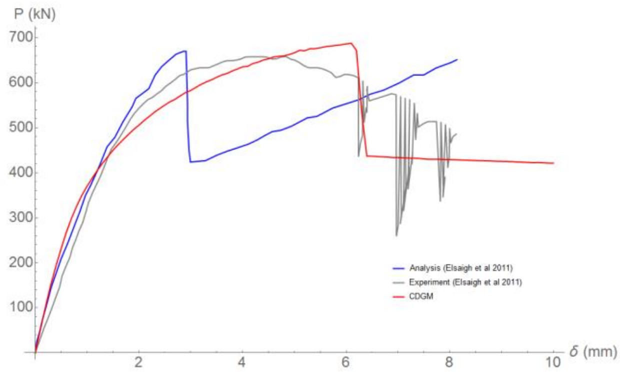

Fig. 13 Problem 2: $P-\delta$ results. Finite element simulation (blue) and experimental data (gray) by Elsaigh *et al*. (2011); CDGM results in red

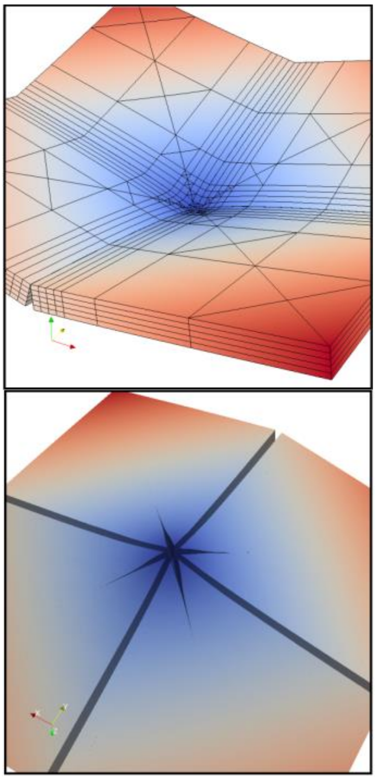

Fig. 14 Problem 2: deformed shape (top and bottom view). Deformation is scaled 20 times for better visualization

only provides vertical forces. In the horizontal directions, a friction factor of 0.1 is adopted, following the same assumption of Elsaigh *et al.* (2011). The load was applied using a hydraulic twin jack bearing on a stiffened loading plate (100×100 mm). The cohesive curve is presented in Fig. 11 where a bilinear curve is adopted. Tension strength is 4.2 MPa and fracture energy is about $G_F = 7000\ \mathrm{J/m^2}$. Additionally, the Mohr-Coulomb yielding criterion is adopted to allow elements in compression to yield.

The mesh is shown in Fig. 12. There are hexahedra and triangular prism elements. Discontinuous elements are blue and continuous elements are depicted in red. Approximation order $p = 2$ is adopted for all continuous elements and $p = 3$ for discontinuous elements. Discontinuous elements are placed in regions where cracks evolve and continuous elements elsewhere. The choice of continuous/ discontinuous elements was made by solving coarser meshes in an adaptive process. A vertical displacement is applied to the steel plate and reaction forces are read. The $P-\delta$ curve is presented in Fig. 13. The CDGM results are compared to the results presented by Elsaigh *et al.* (2011), which includes the experimental data and a finite element simulation. The numerical solutions present a peak load similar to that of the experiment, but the CDGM shows a better agreement with experiments at late stages of loading. Fig. 14 depicts the deformed shape of the ground slab as obtained with the CDGM simulation for a vertical load of $\delta = 10$ mm. The figure shows the crack propagation towards the edges of the slab and in the diagonal directions towards the corners.

5. Conclusions

This paper addresses the application of the continuous-discontinuous Galerkin method (CDGM) to simulate crack propagation in concrete structures. The discontinuous Galerkin method possesses a natural ability to dealing with discontinuities. However, it requires an increased number of degrees of freedom when compared with the classical continuous H^1 finite element method. Therefore, a natural approach is combining both continuous and discontinuous elements in the same simulation obtaining the advantages of both methods.

Two examples of crack propagation are presented. In the first example, a plain concrete beam is tested. The mesh is aligned to the crack path and results are compared to experimental data with good agreement. Results demonstrate the capacities of CDGM to simulate cracking processes using the cohesive fracture model. The cohesive law has strong influence in the results and its definition demands experimental data. In this example, the Hordijk's equation is constructed from the concrete tension strength and its apparent fracture energy. The continuous-discontinuous Galerkin method (CDGM) led to results almost identical to that of the Discontinuous Galerkin method, but with a reduced computational cost. The second example simulates a full-scale steel-fiber reinforced concrete ground slab. A CDGM mesh is proposed and results are compared to numerical and experimental data from the literature. The mesh construction for the CDGM requires the knowledge of crack locations to choose which elements are continuous H^1 and which elements are discontinuous. The elements can be defined by using a prior knowledge of the problem, as in problem 1, or through mesh adaptation, as in problem 2.

Acknowledgments

This research did not receive any specific grant from funding agencies in the public, commercial, or not-for-profit sectors.

References

Asferg, J.L., Poulsen, P.N. and Nielsen, L.O. (2007), "A direct XFEM formulation for modeling of cohesive crack growth in concrete", *Comput. Concrete*, **4**(2), 83-100.

Barenblatt, G.I. (1959), "The formation of equilibrium cracks during brittle fracture. General ideas and hypotheses. Axially-symmetric cracks", *J. Appl. Math. Mech*., **23**, 622-636.

Barenblatt, G.I. (1962), "The mathematical theory of equilibrium of crack in brittle fracture", *Adv. Appl. Mech*., **7**, 55-129.

Cangiani, A., Chapman, J., Georgoulis, E.H. and Jensen, M. (2013), "On the stability of continuous-discontinuous Galerkin methods for advection-diffusion-reaction problems", *J. Scientif. Comput.*, **57**, 313-330.

Cangiani, A., Chapman, J., Georgoulis, E.H. and Jensen, M. (2014), "On local super-penalization of interior penalty discontinuous Galerkin methods", *Int. J. Numer. Anal. Mod*., **11**(3), 478-495.

Dawson, C. and Proft, J. (2002), "Coupling of continuous and discontinuous Galerkin methods for transport problems, Comput", *Meth. Appl. Mech. Eng*., **191**, 3213-3231.

Devloo, P.R.B., Forti, T.L.D. and Gomes, S.M. (2007), "A combined continuous-discontinuous finite element method for convection-diffusion problems", *Latin Am. J. Solid. Struct*., **4**, 229-246.

Dong, Y., Wu, S., Xu, S.S., Zhang, Y. and Fang, S. (2010), "Analysis of concrete fracture using a novel cohesive crack method", *Appl. Math. Model*., **34**, 4219-4231.

Elsaigh, W.A. (2001), "Steel fiber reinforced concrete ground slabs: a comparative evaluation of plain and steel fiber reinforced concrete ground slabs", Master Dissertation, University of Pretoria, South Africa.

Elsaigh, W.A., Kearsley, E.P. and Robberts, J.M. (2011), "Modeling the behavior of steel-fiber reinforced concrete ground slabs. II: Development of slab nodel", *J. Transp. Eng*., **137**, 889-896.

Feng, D.C. and Wu, J.Y. (2018), "Phase-field regularized cohesive zone model (CZM) and size effect of concrete", *Eng. Fract. Mech.*, **197**, 66-79.

Forti, T.L.D., Farias, A.M., Devloo, P.R.B. and Gomes, S.M. (2016), "A comparative numerical study of different finite element formulations for 2D model elliptic problems: Continuous and discontinuous Galerkin, mixed and hybrid methods", *Finite Elem. Anal. Des.*, **115**, 9-20.

Gamino, A.L., Manzoli, O.L, Sousa, J.L.A.O. and Bittencourt, T.N. (2010), "2D evaluation of crack openings using smeared and embedded crack models", *Comput. Concrete*, **7**(6), 483-496.

Hillerborg, A., Modeer, M. and Petersson, P. (1976), "Analysis of crack formation and crack growth in concrete by means of fracture mechanics and finite elements", *Cement Concrete Res.*, **6**, 773-782.

Hordijk, A.D. (1991), "Local approach to fatigue of concrete", Doctoral Thesis, Delft University of Technology, The Netherlands.

Hu, S., Xu, A., Hu, X. and Yin, Y. (2016), "Study on fracture characteristics of reinforced concrete wedge splitting tests", *Comput. Concrete*, **18**(3), 337-354.

Kh, H. M., Özakça, M., Ekmekyapar, T, and Kh, A. M. (2016), "Flexural behavior of concrete beams reinforced with different types of fibers", *Comput. Concrete*, **18**(5), 999-1018.

Kurumatani, M., Soma, Y. and Terada, K. (2019), "Simulations of cohesive fracture behavior of reinforced concrete by a fracture-mechanics-based damage model", *Eng. Fract. Mech.*, **206**, 392-407.

Larson, M.G. and Niklasson, A.J. (2001), "Conservation properties for the continuous and discontinuous Galerkin methods", Tech. Rep. 2000-08, Chalmers University of Technology.

Lin, H.X., Lu, J.Y. and Xu, B. (2017), "Numerical approach to fracture behavior of CFRP/concrete bonded interfaces", *Comput. Concrete*, **20**(3), 291-295.

Murthy, A.R., Ganesha, P., Kumarb, S.S. and Iyerc, N.R. (2015), "Fracture energy and tension softening relation for nano-modified concrete", *Struct. Eng. Mech.*, **54**(6), 1201-1216.

Oden, J.T., Babuska, I. and Baumann, C.E. (1998), "A discontinuous hp finite element method for diffusion problems", *J. Comput. Phys*., **146**, 491-519.

Oden, J.T., Carey, G.F. and Becker, E.B. (1981), *Finite Elements: An Introduction*, Prentice Hall Inc., New Jersey, USA.

Rosa, A.L., Yu, R.C., Ruiz, G., Saucedo, L. and Sousa, J.L.A.O. (2012), "A loading rate dependent cohesive model for concrete fracture", *Eng. Fract. Mech.*, **82**, 195-208.

Santos, F.L.G. and Souza, J.L.A.O. (2015), "Determination of parameters of a viscous-cohesive fracture model by inverse analysis", *Ibracon Struct. Mater. J.*, **8**, 669-706.

Suárez, F., Gálvez, J.C., Enfedaque, A. and Alberti, M.G. (2019), "Modelling fracture on polyolefin fibre reinforced concrete specimens subjected to mixed-mode loading", *Eng. Fract. Mech.*, **211**, 244-253.

Süli, E., Schwab, C. and Houston, P. (2000), "hp-DGFEM for Partial Differential Equations with Nonnegative Characteristic Form". Eds. Cockburn, B., Karniadakis, G.E. and Shu, C.W., Discontinuous Galerkin Methods. Lecture Notes in Computational Science and Engineering, **11**, 221-230.

Yaylacı, M. (2016), "The investigation crack problem through numerical analysis", *Struct. Eng. Mech.*, **57**(6), 1143-1156.

Yu, R.C., Zhang, X. and Ruiz, G. (2008), "Cohesive modeling of dynamic fracture in reinforced concrete", *Comput. Concrete*, **5**(4), 389-400.

CC